Journal of Molecular Catalysis A: Chemical 353–354 (2012) 29–36

Contents lists available at SciVerse ScienceDirect

Journal of Molecular Catalysis A: Chemical

journal homepage: www.elsevier.com/locate/molcata

Photodeposition of Ni nanoparticles on TiO_2 and their application in the catalytic ozonation of 2,4-dichlorophenoxyacetic acid

Julia L. Rodríguez[a,b], Miguel A. Valenzuela[a,*], Francisco Pola[c], Hugo Tiznado[d], Tatiana Poznyak[b]

[a] Lab. Catálisis y Materiales, ESIQIE – Instituto Politécnico Nacional, Zacatenco, 07738 México, D.F. Mexico
[b] Lab. Ing. Química Ambiental, ESIQIE – Instituto Politécnico Nacional, Zacatenco, 07738 México, D.F. Mexico
[c] Centro de Investigación en Materiales Avanzados, Miguel de Cervantes 120, 31109 Chihuahua, Chih., Mexico
[d] Universidad Nacional Autónoma de México, Centro de Nanociencias y Nanotecnología, Km. 107 Carretera Tijuana a Ensenada, C. P. 22860, Ensenada, Baja California, Mexico

ARTICLE INFO

Article history:
Received 23 June 2011
Received in revised form 13 October 2011
Accepted 1 November 2011
Available online 10 November 2011

Keywords:
Ni nanoparticles
Photodeposition
Titanium dioxide
Catalytic ozonation
2,4-D

ABSTRACT

Different photochemical approaches have been investigated to prepare supported nickel nanoparticles to be used in the catalytic ozonation of 2,4-dichlorophenoxyacetic acid (2,4-D). Direct photochemical (λ = 365 nm, without TiO_2) and photocatalytic deposition in presence or absence of sensitizers (TiO_2, acetone or benzophenone) were employed. The characterization of the catalysts was carried out by X-ray diffraction (XRD), X-ray photoelectron spectroscopy (XPS) and transmission electron microscopy (TEM). The photocatalytic deposition without any sensitizer resulted to be the most suitable method to obtain in very short irradiation time, Ni nanoparticles randomly distributed over the support with a particle size ranging from 7 to 15 nm. An optimization of this technique was performed by varying the mass of TiO_2 and the light intensity. According to the results of 2,4-D degradation, the catalytic ozonation with Ni/TiO_2 catalyst presented a slightly higher conversion than TiO_2 or ozonation alone. These results were explained in terms of the two phases (NiO/Ni) present on the surface of TiO_2 which favor the ozone decomposition forming OH radicals useful for 2,4-D degradation. A reaction pathway including all the intermediates formed during the direct attack of ozone and the produced OH radicals was proposed.

1. Introduction

There is a growing need for understanding the mechanisms for catalytic ozonation to introduce this technique in water treatment at industrial scale [1–3]. Current research has been divided into two routes, homogeneous and heterogeneous catalytic ozonation. Concerning the last route, several catalysts have been tested, including metal oxides, metals on supports, minerals and activated carbon, among others [3]. The catalytic ozonation can proceed by direct molecular ozone reactions and by an indirect pathway forming OH radicals after ozone decomposition. However, the ozonation process alone has its limitations, and the most important is that the total mineralization of toxic organic compounds is difficult to achieve. Therefore, the presence of a catalyst in the ozonation process improves and controls the ozone decomposition and OH radicals formation leading to mineralization [3].

In recent years, several researchers have reported on the degradation of organic pollutants by the heterogeneous catalytic ozonation using TiO_2 [4–6], NiO unsupported and supported [7–9] and other metal oxides [10,11], however, a general conclusion about the reactivity with each kind of catalyst is not clear yet. In contrast, supported metal catalysts have been scarcely studied specifically in the effect of the preparation method on the degradation performance. In particular, if supported metal catalysts are employed in the catalytic ozonation of contaminants is thought that two reaction mechanisms can occur. By the first mechanism, organics are adsorbed on the surface of the catalyst and then attacked by ozone or hydroxyl radicals; by the second mechanism, both ozone and organics adsorb on the surface of the catalyst and a redox process takes place forming organic radicals that are subsequently oxidized by hydroxyl radicals or ozone [1,3].

As is well known, the catalyst preparation method plays an important role in the size, morphology and particle size distribution [12]. In fact, during the last two decades, several synthetic methods such as chemical, thermal, photochemical, radiation, among others, have been used in the preparation of metallic or metal oxide nanoparticles [13–16]. According to our previous works, a photodeposition method ensures the formation of small Pt particles (2–4 nm) supported on C or TiO_2 with a narrow particle size distribution [17,18]. In a general way, the photodeposition process takes place when the chromophore of a complex absorbs a photon resulting in a photoexcited state, then, the complex may decompose by a photoredox reaction to produce a solid metallic phase cluster able to deposit over the substrate surface [19–23]. The photodeposition

* Corresponding author. Tel.: +52 55 57296000x55112.
E-mail address: mavalenz@ipn.mx (M.A. Valenzuela).

1381-1169/$ – see front matter © 2011 Elsevier B.V. All rights reserved.
doi:10.1016/j.molcata.2011.11.001

method is reproducible and the reaction can be stopped at any time by switching the lamp off. However, byproducts coming from the solvent oxidation/decomposition reactions can be generated after irradiation [24].

Diverse catalysts based on supported nickel have been used in chemical processes industrially important, including hydrogenation, methanation, reforming, dechlorination, desulfurization, and so on. These catalysts are generally synthetized by impregnation or coprecipitation with nickel salts on a support [25]. Nevertheless, it presents the problem of formation of mixed nickel oxides, especially for nickel loadings of 10 wt% and high calcination temperatures (≥600 °C), which are required to completely reduce the Ni(II) cations to metallic nickel particles, which leads to the unwanted metal sintering [26]. Therefore, one of the main advantages of the photodeposition method is the direct reduction of the Ni precursor avoiding reductive thermal treatments. Works devoted to the photodeposition of Ni nanoparticles on semiconductors are scarce and the effect of synthesis parameters has not been reported yet [27].

In this study, we have explored the use of TiO_2 to promote the photocatalytic deposition of Ni nanoparticles. The nickel (II) present in the precursor solution is reduced with the photogenerated electrons on the TiO_2 surface. Additionally, an easily oxidable compound (e.g. ethanol) must be present in the system to assure that holes are consumed to avoid their accumulation on the photocatalyst surface, which could stop the photocatalytic activity or cause nickel reoxidation [28,29]. It seems that the addition of oxalate ion as a co-reactant favors the reduction of nickel (II) on TiO_2 by an indirect photoreduction in aqueous solution [27].

The evaluation of our photodeposited Ni/TiO_2 catalysts was carried out in the degradation of herbicide 2,4-dichlorophenoxyacetic acid (2,4-D) by heterogeneous catalytic ozonation in aqueous solution. 2,4-D was selected as a model compound, since it is the most widely used in agriculture sector and herbicide in the world, it is poorly biodegradable and has been detected as a major pollutant in ground and surface water [30].

2. Experimental

2.1. Materials and reagents

The bis(2,4-pentandionato) Ni(II) (Ni(acac)$_2$, Aldrich) was reagent grade. Anhydrous ethanol and acetone (J.T. Baker) were spectrophotometric grade. TiO_2 powder P25 (Degussa AG, 80% anatase and 20% rutile, non-porous, BET surface area = 44 $m^2\,g^{-1}$) was used as starting material. 2,4-dichlorophenoxyacetic acid (Alfa Aesar, 90%) and benzophenone (Aldrich, analytical grade) were used as received.

2.2. Catalyst preparation

In a glass reactor, it was added a TiO_2 (0.1 g) suspension containing a 8×10^{-4} M alcoholic solution of Ni(acac)$_2$ at 25 °C to have a total volume of 100 mL, purged with nitrogen. The mixture was irradiated with 14 black light UVA lamps (8 W) with a maximum emission at about 365 nm. The sensitized photoreaction was performed in presence of acetone (0.2 M) or benzophenone (10^{-3} M). The suspension was subjected to vigorous and continuous stirring to avoid both the film formation and sedimentation of TiO_2. After irradiation, the sample was dried at 120 °C to evaporate the solvent. The kinetics of the Ni(acac)$_2$ photodecomposition was performed by using a Lambda UV–Vis spectrophotometer (Perkin Elmer) at wavelength of 310 nm.

2.3. Characterization techniques

The specific surface area of the supported catalyst Ni/TiO_2 and the TiO_2 support were determined by the BET method of nitrogen adsorption using a MicromeritisAutochem II 2920. Metal content in the prepared catalyst was obtained using an atomic absorption spectrophotometer (Perkin Elmer). XRD patterns were obtained in a XïPert-P analytical diffractometer with a Cu source ($\lambda K\alpha$ = 0.15418 nm) and operated at 40 kV and 35 mA. The instrument was coupled with a nickel filter and a X'Celerator detector and it was settled in tetha/2tetha configuration. The scanning angle (2θ) range was varied to 20–90° with 0.016 step size and 20 s of counting time. Phase analysis was carried out matching diffracted intensities with PDF cards.

TEM images were obtained using a JEOL-JEM-2200 field emission operated at 200 kV. The samples were prepared with the catalyst (<1 mg) in methanol and dispersed by ultrasound for 5 min. Thereafter, a drop of the solution was placed over a carbon coated Cu grid (300 mesh) and dried at room temperature. Photoelectron core-level spectra of the as-prepared samples were obtained with an X-ray photoelectron spectroscopy (XPS) system (Riber LDM-32), which has an analysis chamber equipped with an ion pump, an electron-energy analyzer (Mac-3) and a dual anode X-ray source. XPS data were collected using the Al Kα line at 1486.6 eV. The high resolution XPS scans were completed at 0.1 eV energy steps and 0.5 eV resolution (~25 eV pass energy), while the surveys at 1 eV steps and 3 eV resolution (~100 eV pass energy). The spectra were decomposed into their components with mixed Gaussian–Lorentzian lines by a non-linear least squares curve-fitting procedure, using the public software package XPSPEAK 4.1. The binding energies and FWHM of the peaks were determined from the fitting results after subtraction of the Shirley-type background. Deconvoluted peak areas and standard sensitivity factors were used to evaluate the surface composition of the samples.

2.4. Ozone generation and ozone consumption control

Ozone was generated from dry oxygen by the ozone generator (corona discharge type) HTU500G (AZCO Industries Limited – Canada). The Ozone Analyzer BMT 964 BT (BMT Messtechnik, Berlin) provides the ozone monitoring in the gas phase at the reactor outlet for the control of the ozonation degree, the ozone consumption and the ozone decomposition as well.

2.5. Ozonation procedure

All experiments with ozone were carried out in a semi-batch type reactor (0.5 L) at 21 °C. The agitation was provided by means of an ozone–oxygen mixture bubbling through a ceramic porous filter, which is placed at the bottom of the reactor. The initial ozone concentration was 25 mg L^{-1}. The ozone–oxygen mixture flow was 0.5 L min^{-1}. A flow diagram showing the ozonation procedure and equipment is depicted in Fig. 1.

The model solution of 2,4-D herbicide was prepared with a concentration of 80 mg L^{-1}. Aliquot of 3-mL ozonation reaction solution was withdrawn at time intervals from the reactor for sequent analysis. The catalyst concentration was 0.1 g L^{-1}.A HPLC apparatus (Perkin-Elmer series 200, UV/Vis detector) was used to record the change of concentration of 2,4-D, under the following operation conditions: column Prevail Organic Acid 5 μ "Grace", 150 × 4.6 mm with 60:40 acetonitrile–buffer mobile phase of KH_2PO_4 at 25 mM adjusted a pH 2.6 with H_3PO_4 at wavelength 225 nm with the flow 1 mL min^{-1}.

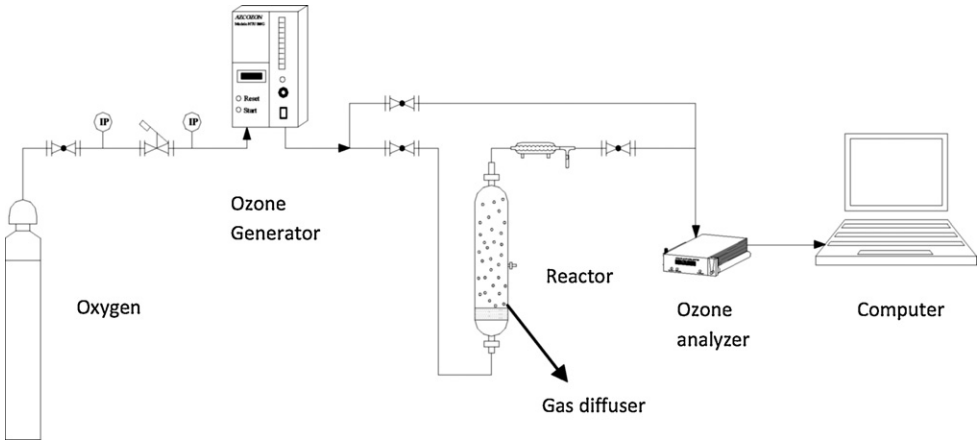

Fig. 1. Schematic diagram of the ozonation apparatus.

3. Results and discussion

3.1. Photochemical reaction

The evolution of the $Ni(acac)_2$ normalized concentration as a function of irradiation time is compared in Fig. 2. As can be seen, a negligible decomposition of $Ni(acac)_2$ is observed after 6 h of irradiation time without the presence of a sensitizer, which means that the photoexcitation of the Ni precursor did not occur at the wavelength used in the experiment ($\lambda = 365$ nm). However, in presence of acetone or benzophenone, a mild conversion of the Ni precursor is detected. Indeed, several researchers have reported that acetone and mainly aromatic ketones improve the photochemical decomposition of metal complexes by sensitization [31,32].

The photochemical reduction has already been reported and this reaction can proceed by the following mechanism (Scheme 1) [33]:

The photodecomposition rate of $Ni(acac)_2$ in ethanol at 365 nm is very low because only 1% $Ni(acac)_2$ is decomposed in 6 h (Fig. 2). This low photodecomposition rate can be increased by using the "acetone method", which has been proved successfully in the formation of Ag nanoparticles [34,35]. Therefore, two photosensitizers acetone (AC) and benzophenone (BP) were tested in the photodecomposition of $Ni(acac)_2$. A beneficial behavior was observed with acetone and the decomposition rate is increased in 18% in 6 h of irradiation time, while by using benzophenone the same decomposition degree was obtained but just in 1 h. This photosensitized reduction uses the photoactive reagents (e.g. benzophenone,) generating intermediates after UV irradiation, which reduce the metal precursor to its metallic form [24]. Furthermore, when the photodecomposition reaction proceeds in presence of any sensitizer, the solution color turned form light green to dark brown. This change in the $Ni(acac)_2$ solution color has been attributed to the formation of nickel colloidal particles [21,36].

The kinetic analysis of the photochemical reaction with or without sensitizers is also presented in Fig. 2. It is clearly shown that the raw data fitted well to a first order kinetics. Note that in presence of BP, the rate constant ($k = 0.17\ h^{-1}$) was one magnitude order higher with respect to the rate constant in presence of AC ($k = 0.03\ h^{-1}$). The photochemical reaction, without any sensitizer, was very low with a rate constant of $k = 0.0078\ h^{-1}$. The improved reaction rate obtained by the addition of BP may be due to the electron transfer reaction between the sensitizer and the Ni precursor as shown in the following reactions (Scheme 2) [37].

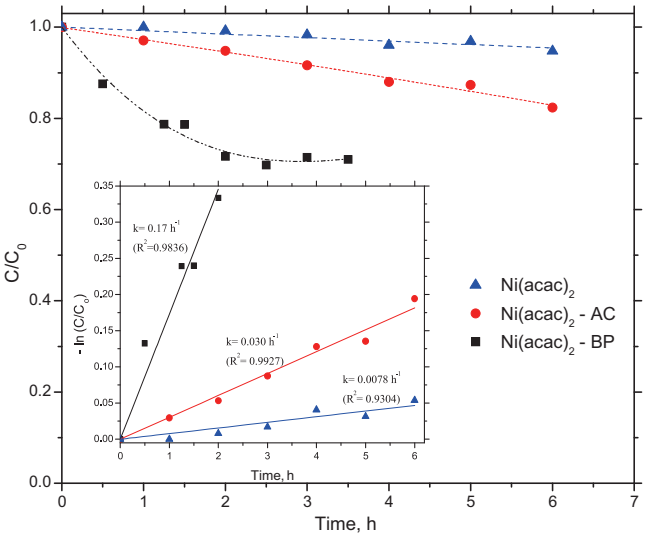

Fig. 2. Evolution of the dimensionless concentration of $Ni(acac)_2$ with irradiation time in presence of sensitizer (AC – acetone; BP – benzophenone) and without it. Experimental conditions: $[Ni(acac)_2] = 8 \times 10^{-4}$ M, [AC] = 0.2 M, [BF] = 10^{-3} M, $\lambda = 365$ nm. Insert kinetic analysis assuming a first order reaction.

3.2. Photocatalytic reaction

The photocatalytic deposition of Ni nanoparticles, employing $Ni(acac)_2$ in ethanol solution (as sacrificial electron donor) was carried out in presence of sensibilizer and without it, the results are shown in Fig. 3. The presence of TiO_2 in the reaction lead to a rapid reduction of the Ni precursor compared with the photochemical reduction. As it is known, the conduction band electrons on the surface of a TiO_2 particle has a reduction potential of −0.5 V (vs. NHE at pH = 7), then, it can reduce Ni ions because their redox potential Ni^{2+}/Ni is −0.24 V [38]. However, it has been suggested that an overpotential of 0.3 V is required for an efficient reduction. As can be seen in Fig. 3, the nickel reduction was at about 90% after 1.5 h of irradiation time, and then no more reduction was observed. The presence of either sensitizer presented a much lower conversion of the Ni precursor, mainly at low irradiation times (0–2 h). Probably, after the adsorption of BP and AC on the surface of TiO_2 hinder the photons absorption by the semiconductor.

The dimensionless residual concentration of $Ni(acac)_2$ as a function of the incident light intensity after 1.5 h of irradiation is shown in Fig. 4. Note that the tendency of the concentration profiles with or without sensitizer was similar, practically linear in all the range of light intensity. Nevertheless, the photocatalytic deposition of Ni nanoparticles on TiO_2 without sensitizer was always higher. An explanation of this behavior can be due to a competition for the

$$Ni(acac)_2 \xrightarrow{h\nu} Ni^0 + Hacac + \text{decomposition products of the solvent} \quad (1)$$

$$Ni(acac)_2 + CH_3—CH_2—OH \xrightarrow{h\nu, N_2} Ni(acac) + Hacac + CH_3—C\cdot HOH \quad (2)$$

$$Ni(acac) \longrightarrow Ni^0 + acac\cdot \quad (3)$$

$$acac\cdot + CH_3—CH_2—OH \longrightarrow Hacac + CH_3—C\cdot HOH \quad (4)$$

$$2\,CH_3—C\cdot HOH \longrightarrow CH_3—CH_2—OH + CH_3—CH=O \quad (5)$$

Scheme 1.

$$R_2C=O \xrightarrow{h\nu} {}^1R_2C=O \xrightarrow{h\nu} {}^*R_2C=O \quad (6)$$

$${}^*R_2C=O + Ni(acac)_2 \longrightarrow \left[{}^*R_2C=O^{\cdot-} \text{ --- } Ni(acac)_2^{\cdot+}\right] \quad (7)$$

$$\left[{}^*R_2C=O^{\cdot-} \text{ --- } Ni(acac)_2^{\cdot+}\right] \longrightarrow \left[{}^*R_2C=O^{\cdot-} \text{ --- } Ni(acac)^{+} \text{ --- } acac\cdot\right] \quad (8)$$

$$\left[{}^*R_2C=O^{\cdot-} \text{ --- } Ni(acac)^{+} \text{ --- } acac\cdot\right] \longrightarrow R_2C=O + Ni(acac) + acac\cdot \quad (9)$$

$$Ni(acac) \longrightarrow Ni^0 + acac\cdot \quad (10)$$

$$acac\cdot + CH_3—CH_2—OH \longrightarrow Hacac + CH_3—C\cdot HOH \quad (11)$$

$$2\,CH_3—C\cdot HOH \longrightarrow CH_3—CH_2—OH + CH_3—CH=O \quad (12)$$

Scheme 2.

incident photons by the TiO_2 and the sensitizer. Indeed, as the wavelength of the lamps used in our experiments was centered at 365 nm, then, higher photons absorption must take place with the TiO_2 than with the organics.

To clarify the behavior shown in Fig. 4, data concerning to the evolution of the Ni $(acac)_2$ as a function of irradiation time at several light intensities are shown in Fig. 5. The curves exhibited a reverse S-shaped form with three well-defined sections; Section I corresponds to an induction period with the nickel precursor decomposition giving rise to a small absorption change. The length of the induction period depends inversely on the light intensity. During this time begins the photoreduction of Ni(II) complex to intermediate species, including Ni(I) and Ni(0). The significant shift in the $Ni(acac)_2$ photodecomposition is observed in Section II causing the reduction of Ni(II) adsorbed on TiO_2. The tendency to achieve a plateau in the kinetic curve in Section III could be indicative that the reduction of Ni(II) was completed. As a consequence, the intensity of light that penetrates deep into the TiO_2 gradually falls and the nickel photodecomposition did not present variations with irradiation time.

The effect of the TiO_2 concentration on the photoreduction of $Ni(acac)_2$ in ethanol was also studied and reported in Fig. 6. These results indicated the expected trend: the higher the TiO_2 concentration, the higher conversion of the $Ni(acac)_2$. According to these results, an optimal concentration of TiO_2 was reached at about 1 g L^{-1}. Most studies reported that a enhanced degradation rates are obtained for catalyst loads up to 0.4–0.5 g L^{-1} [32]. This behavior can be explained in terms of the availability of active sites on the TiO_2 surface and the light penetration into the suspension. Indeed,

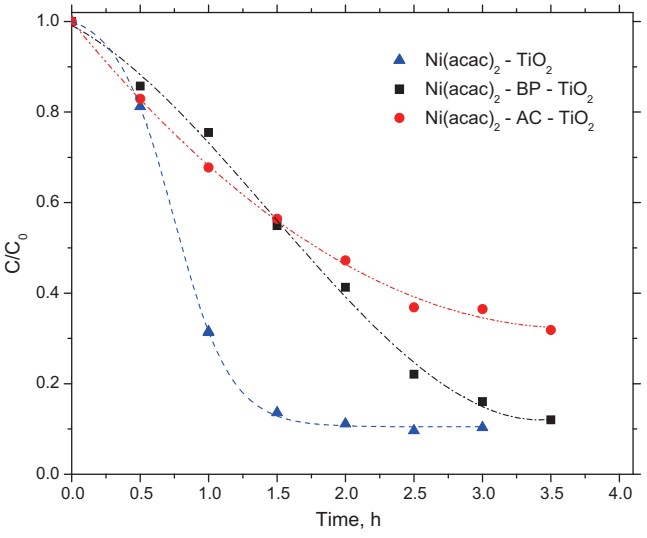

Fig. 3. Evolution of the dimensionless concentration of nickel reduction with irradiation time at 365 nm. Experimental conditions: $[Ni(acac)_2] = 8 \times 10^{-4}$ M, [AC] = 0.2 M, [BF] = 10^{-3} M, λ = 365 nm, $[TiO_2] = 1.075$ g L^{-1}.

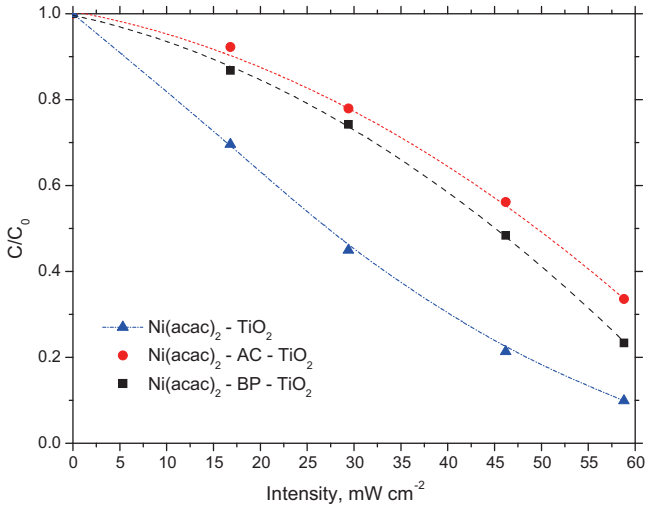

Fig. 4. Evolution of the dimensionless concentration of the photocatalytic reduction of $Ni(acac)_2$ as a function of light intensity. Experimental conditions: $[Ni(acac)_2] = 8 \times 10^{-4}$ M, λ = 365 nm, $[TiO_2] = 1.075$ g L^{-1}.

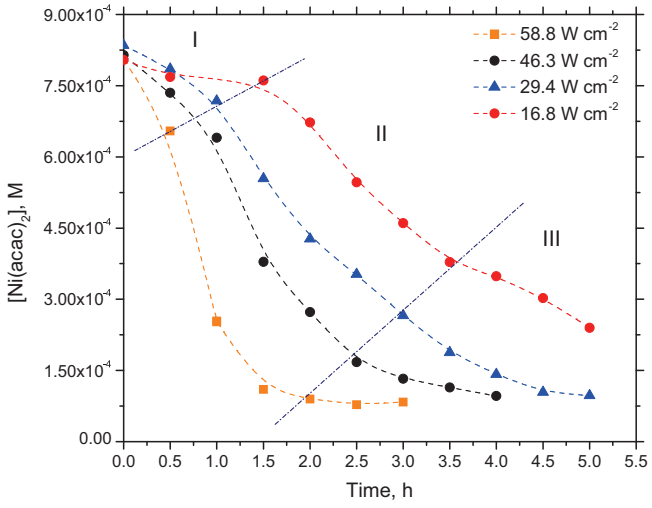

Fig. 5. Evolution of the $Ni(acac)_2$ concentration as a function irradiation time with respect a different light intensity. Experimental conditions: $[Ni(acac)_2] = 8 \times 10^{-4}$ M, $\lambda = 365$ nm, $[TiO_2] = 1.075\ g\ L^{-1}$.

there is a limit of catalyst loading in which agglomeration and sedimentation dominate and the catalyst surface became unavailable for photon absorption and adsorption of the reactant. The optimum loading of photocatalyst depends on the geometry of the reactor, the type of UV-lamp, the operational conditions of the reactor and of course on the initial solute concentration [39]. Note that the estimated initial reaction rates against TiO_2 agreed very well to a first order kinetics in the inserted plot in Fig. 6.

3.3. Catalyst characterization

The real nickel content on TiO_2 was 3.6 wt%, compared with a nominal amount of 5 wt%, which confirms that some of the Ni precursor is maintained in solution without further reduction. Nitrogen physisorption results (not shown here) indicated that TiO_2 had major specific surface area (SSA 44 $m^2\ g^{-1}$) compared with that of Ni/TiO_2 (33 $m^2\ g^{-1}$), this reduction in SSA is due to the blockage of the pores support during the deposition reaction. The IEP

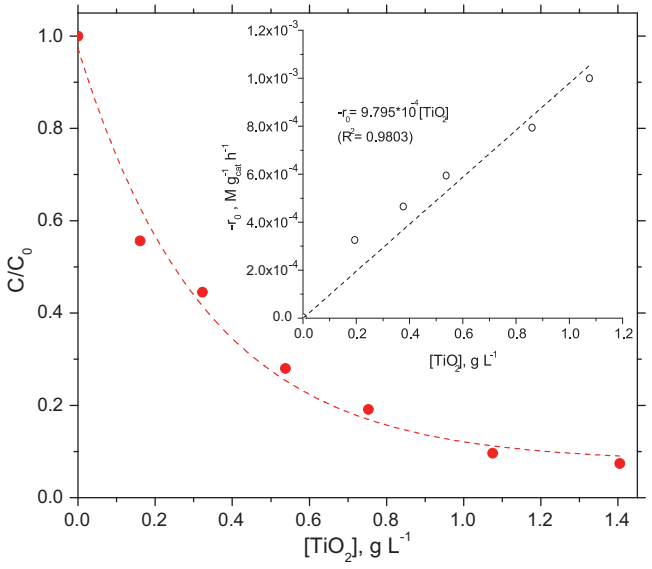

Fig. 6. Evolution of the dimensionless concentration of nickel reduction with TiO_2 loading and its relation with initial rate reaction. Experimental conditions: $[Ni(acac)_2] = 8 \times 10^{-4}$ M, $\lambda = 365$ nm. Insert kinetic analysis.

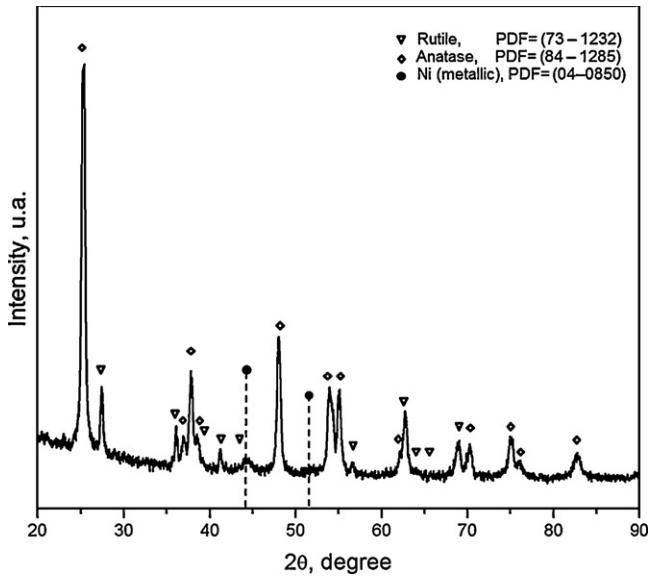

Fig. 7. Diffraction pattern of Ni/TiO_2 sample.

value of Ni/TiO_2 was 6.09 and for TiO_2 was 6.46 so that the presence of nickel did not change significantly the isoelectric point. H_2 chemisorption data show a dispersion of 6.5% which correspond to an average particle diameter of 16.5 nm. Comparable values of average Ni size diameters have been obtained from TEM analysis ($d_{TEM} \approx 13$ nm).

Fig. 7 shows the XRD pattern of Ni/TiO_2 synthesized by the photocatalytic deposition method. The XRD pattern of Ni/TiO_2 sample evidence TiO_2 rutile and anatase phases with tetragonal structures, identified with PDF cards (73–1232) and (84–1285), respectively. Lattice parameters of semiconductor phases were $a = b = 0.45936$ nm and $c = 0.29587$ nm for rutile and $a = b = 0.37848$ nm and $c = 0.9512$ nm for anatase. In the Ni/TiO_2 sample, Ni^0 phase was observed at $2\theta = 44.34^\circ$, identified as (1 1 1) plane of Ni cubic structure ($a = 0.35238$ nm) according to PDF card (04-0850).

Fig. 8 reports TEM images with different magnification of the sample prepared by photocatalytic deposition. TEM micrographs (Fig. 8a and b) show Ni aggregates deposited over the crystalline TiO_2 semiconductor. Aggregates are formed with Ni nanoparticles ranging from 7 to 15 nm in size although not well defined geometrical shape (see Fig. 8a). Apparently, small Ni nanoparticles are formed in situ during the reaction and are well dispersed in alcoholic media; however, during evaporation and sedimentation steps, the particles aggregate fall down locally over TiO_2. Then, the deposition of Ni particles is not homogeneous over the semiconductor surface. Micrograph of Fig. 8c shows regions of high concentrations of Ni rather than individual metallic particles.

The chemical nature of the Ni-containing catalyst has been investigated with XPS analysis. The spectra were charge corrected using the Ti $2p_{3/2}$ peak position (459.5 eV for TiO_2) [40], as the C 1s signal was composed by several peaks. In a survey spectrum (not shown) there were found signals only for Ni, O, Ti and C, as expected. The corresponding high resolution regions are presented in Fig. 9.

The Ti $2p_{3/2}$ region can be fitted with one peak (FWHM 1.6 eV), indicating a single Ti chemical specie. The C 1s peak is fitted with three peaks. The first one at 284.5 eV is assigned to adventitious carbon. The other two peaks at 286.0 and 288.4 eV are assigned to organic carbon with increasing grade of oxidation [40–42]. The presence of the organic carbon indicates that the reaction byproducts were not removed completely after drying of the sample and/or incomplete Ni precursor decomposition. The 38% of the O 1s

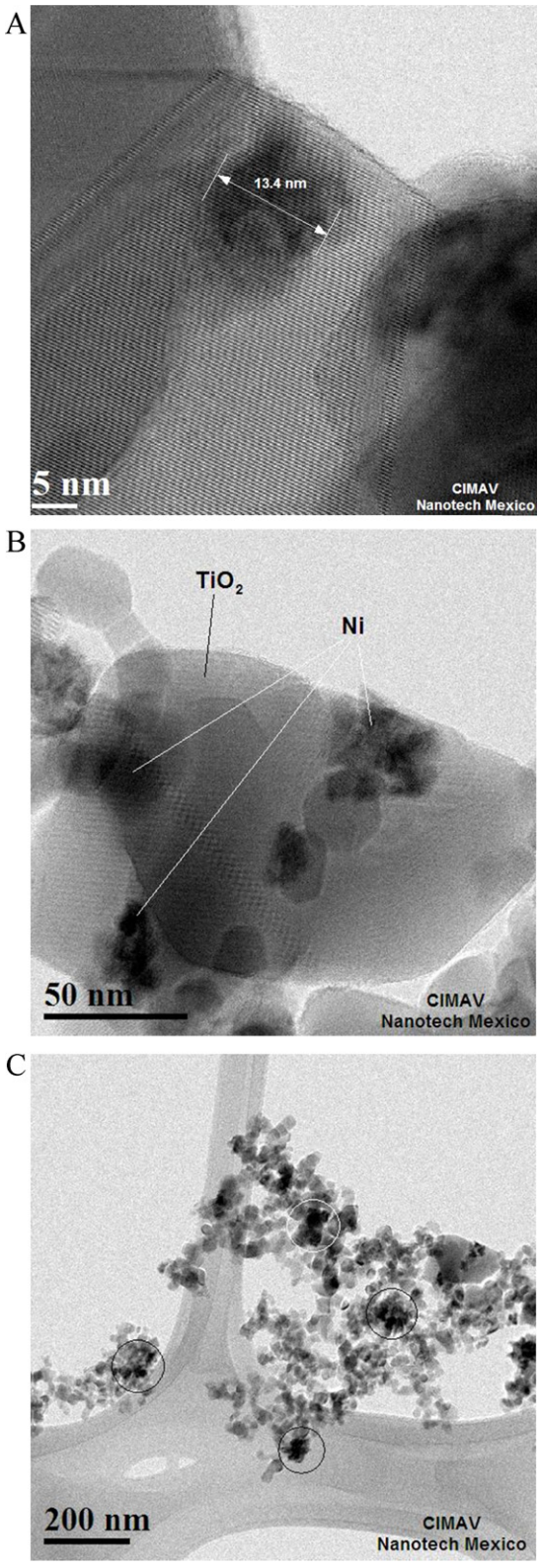

Fig. 8. TEM micrographs of Ni/TiO_2 catalyst prepared by photocatalytic method: (a) and (b) low magnification images; (c) high resolution.

region is composed by a peak at 531.0 eV for O^{2-} species ascribed to TiO_2. The remaining fraction of the peak is fitted by wide peaks at 532.6 and 533.9 eV, FWHM 3.0 and 2.5, respectively. These positions correspond to O- (OH^-) and H_2O adsorbed on the surface, which is typical for titanium oxides [43]. It is clear that there is a contribution of more O peaks, perhaps the extra O is bonded to the organic carbon and to the Ni oxide found in the sample, see below. However, with the current data resolution it is not possible to further deconvolute this peak to propose the positions of the extra O peaks.

The signal-to-noise ratio of the Ni 2p spectral region was poor at the acquired resolution, despite the long period of data collection and does not allows for a reliable interpretation. In order to improve the peak intensity, we opted to acquire a slightly lower resolution spectrum only for the Ni 2p region, which is shown instead of the high resolution one. Nevertheless, it can be extracted valuable information. There are two main peaks at 855.8 and 873.5 eV corresponding to Ni $2p_{3/2}$ and $2p_{1/2}$, respectively. On the HBE side of each main peak appears a satellite shoulder (approximately at 861.5 and 881.0 eV), which intensity, respect to the corresponding main peak, is the distinctive feature of oxidized nickel, i.e. NiO [36,44,45]. Additionally, it can be seen a small shoulder approximately at 852.0 eV corresponding to metallic Ni. Since the nickel oxide 2p region shape is complex (due to the presence of two satellites, which shape is non symmetrical), and given the lack of spectral resolution we consider adventurous trying to deconvolute the peaks, and no atomic percents for NiO or metallic Ni are calculated. Still, given the observed intensities, NiO is the main component in the sample, and the overall nickel concentration is ~6 atomic % in respect to titanium. Nickel nanoparticles on TiO_2 formed after photocatalytic reduction may be accompanied by an oxidation process with atmospheric oxygen. Indeed, in our catalysts it was evident this behavior and we detected metallic nickel by XRD (Fig. 7) and NiO by XPS (Fig. 9d). These results agreed with those reported for several supported nickel catalysts where the uppermost surface of nickel nanoparticle is reoxidized easily as shown by XRD and XPS studies [46,47].

3.4. Catalyst evaluation

Fig. 10 shows the degradation of 2,4-dichlorophenoxyacetic acid (2,4-D) in conventional and catalytic ozonation with TiO_2 and Ni/TiO_2 catalysts at pH 2.5. It is clear that the degradation profiles for simple and catalytic ozonation with TiO_2 were similar, reaching a 50% conversion of the pesticide in 5 min. The activity of the Ni/TiO_2 catalyst was slightly higher and the time required to obtain a 50% conversion of 2,4-D was lower (3.8 min). Obviously, the higher initial reaction rate with the Ni/TiO_2 catalyst indicates that the presence of NiO/Ni active sites on the surface of the TiO_2 can improve the formation of OH radicals used by the degradation of 2,4-D (see attached plot in Fig. 10). Similar results have been reported earlier by using manganese oxides supported on mesoporous zirconia as catalyst and 2,4-D as a model compound [48]. To be more precise, the catalytic ozonation of organic compounds carried out in presence of supported Ni species promotes the ozone decomposition producing a high amount of OH radicals useful for the degradation reactions [7,8]. Therefore, if we assume that our catalytic system Ni/TiO_2 contains a surface layer of NiO and metallic bulk nickel converting at short reaction times (10 min) almost 88% of 2,4-D, then, these two phases (NiO/Ni) could play an important role in the OH radical formation. In particular, our results indicated that catalytic ozonation effectively decomposes O_3 into OH, which confirms what has been reported before [49,50]. Hence, a possible reaction mechanism for ozone decomposition should include a first step for ozone adsorption on the surface of the catalyst and a second one consisting in desorption of the intermediates compounds formed.

With regard to the intermediates formed after conventional and catalytic ozonation with Ni/TiO_2 catalyst, we found 2,4-dichlorophenol (2,4-DCP), glycolic, glyoxylic, maleic, fumaric and oxalic acids. The evolution of the concentration of these compounds (not shown here) during simple or catalytic ozonation was the

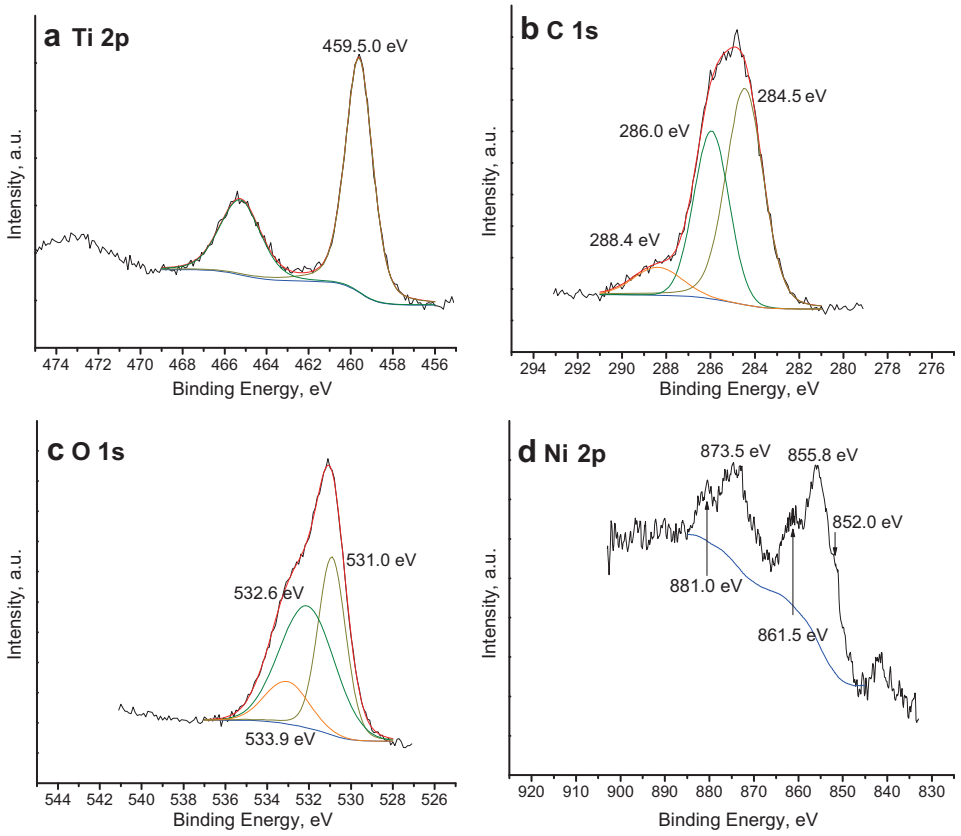

Fig. 9. High resolution XPS spectra of a Ni/TiO_2 sample obtained by photocatalytic process: (a) Ti 2p, (b) C 1s, (c) O 1s and (d) Ni 2p.

same, however the yield of the intermediates by the second route was lower compared with ozonation alone [51]. These results indicated that ozonation and catalytic ozonation had a similar reaction pathway. Therefore, the degradation process of 2,4-D is initiated by the attack of ozone and/or OH radicals on the C(1)–O bond 2,4-D on the aromatic ring to give 2,4-DCP and glycolic acid, as shown in Fig. 11. Particularly, no other aromatic compounds different than 2,4-dichlorophenol were detected by ozonation and

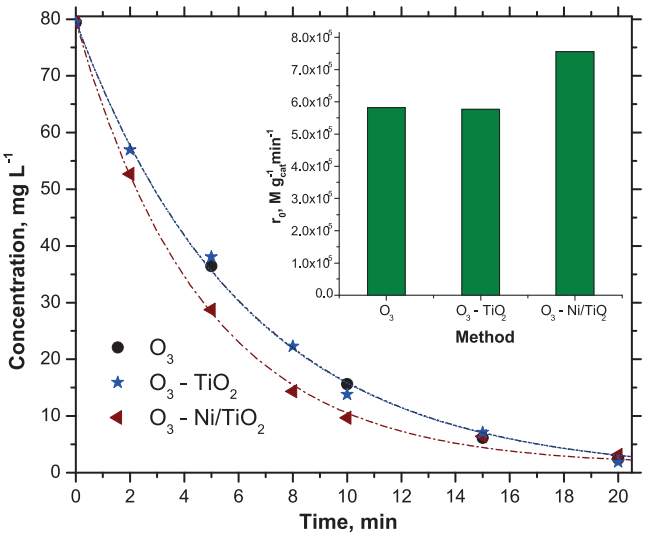

Fig. 10. Decomposition dynamics of 2,4-D in the conventional and catalytic ozonation processes: $[O_3] = 25\ mg\ L^{-1}$, catalyst dose = $0.1\ g\ L^{-1}$, $[2,4\text{-D}] = 80\ mg\ L^{-1}$, pH = 2.5. Insert initial rate reaction as a function of method used in the 2,4-D elimination.

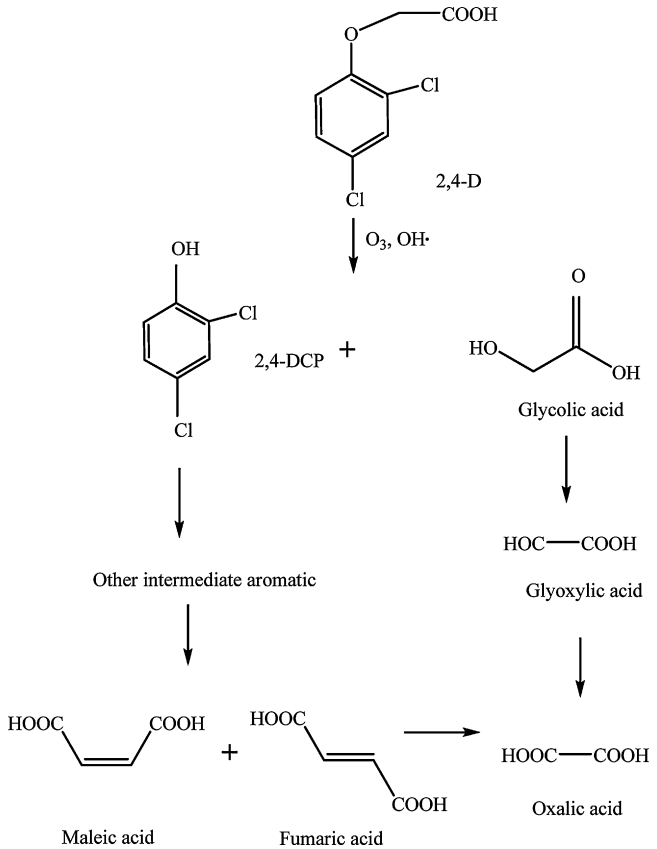

Fig. 11. Suggested reaction pathway for 2,4-D by O_3 and ozonation catalyzed with TiO_2 and Ni/TiO_2 at pH 2.6.

catalytic ozonation. However, if there their decomposition can produce maleic and fumaric acids, which are oxidized to oxalic acid. Alternatively, oxalic acid can also be produced from glycolic acid following a parallel path. Considering that the final byproduct of the whole process was oxalic acid by the two routes, a complete mineralization of 2,4-D did not occur. Nevertheless, due to the amount of intermediate compounds was lower by the catalytic process, it is clear that the partial mineralization of 2,4-D was improved in comparison with the ozonation alone.

4. Conclusion

We developed a procedure to obtain TiO_2 supported-nickel nanoparticles by a photocatalytic deposition route. The Ni precursor was easily reduced at room temperature by the photocatalytic route in comparison with a photochemical method in presence of different sensibilizers. Almost 90% of the Ni precursor was obtained at short reaction time (1.5 h). The photocatalytic deposition was dependent on the light intensity and TiO_2 loading, best results were found at medium intensities (40–60 mW cm^{-2}) and mass of catalyst at about 1 g L^{-1}. It seemed that these experimental conditions allowed optimal photon absorption avoiding electron-hole recombination and agglomeration or sedimentation of TiO_2.

Nickel nanoparticles ranging from 7 to 15 nm (TEM results) were deposited on TiO_2 without any thermal treatment (i.e. hydrogen reduction) which is advantageous compared with the conventional methods. XPS and XRD results evidenced the presence of metallic Ni nanoparticles and nickel oxide. Ni nanoparticles were randomly distributed on the support an easily reoxidized to NiO after stay in contact with atmospheric air. There was no difference in the activity results of ozonation alone compared with catalytic ozonation with TiO_2. However, the presence of two phases (NiO/Ni) in the Ni/TiO_2 improved slightly the conversion of 2,4-D compared with the other routes. It was proposed a reaction path including all the intermediates detected which were formed during the attack of both ozone and OH radicals. It seemed that a higher partial mineralization of 2,4-D was reaching by using catalytic ozonation with the Ni/TiO_2 catalyst.

Acknowledgements

The authors are grateful for the financial support provided by CONACYT (Project Nos. 83275, 49367 and 153356) and PAPIIT IN114209.

References

[1] B. Legube, N. Karpel VelLeitner, Catal. Today 53 (1999) 61–72.
[2] B.K. Hordern, M. Ziółek, J. Nawrocki, Appl. Catal. B: Environ. 46 (2003) 639–669.
[3] J. Nawrockia, B.K. Hordern, Appl. Catal. B: Environ. 99 (2010) 27–42, and references therein.
[4] F.J. Beltrán, F.J. Rivas, R. Montero-de-Espinosa, Appl. Catal. B: Environ. 47 (2004) 101–109.
[5] Y. Yang, J. Ma, Q. Qin, X. Zhai, J. Mol. Catal. A: Chem. 267 (2007) 41–48.
[6] F.J. Beltrán, F.J. Rivas, R. Montero-de-Espinosa, Appl. Catal. B: Environ. 39 (2002) 221–231.
[7] X. Zhang, X. Li, W. Qin, Chem. Phys. Lett. 479 (2009) 310–315.
[8] S.M. Avramescu, C. Bradu, I. Udrea, N. Mihalache, F. Ruta, Catal. Commun. 9 (2008) 2386–2391.
[9] C. Bradu, L. Frunza, N. Mihalche, S.M. Avramescu, M. Neaţă, I. Udrea, Appl. Catal. B: Environ. 96 (2010) 548–556.
[10] L. Zhao, Z. Sun, J. Ma, Environ. Sci. Technol. 43 (2009) 4157–4163, and references therein.
[11] T. Zhang, J. Ma, J. Mol. Catal. A: Chem. 279 (2008) 82–89.
[12] J.F. Lambert, M. Che, J. Mol. Catal. A: Chem. 162 (2000) 5–18.
[13] N. Toshima, T. Yonezawa, New J. Chem. 22 (1998) 1179–1201.
[14] A. Roucoux, J. Schulz, H. Patin, Chem. Rev. 102 (2002) 3757–3778.
[15] B.L. Cushing, V.L. Kolesnichenko, C.J. O'Connor, Chem. Rev. 104 (2004) 3893–3946.
[16] J.A. Dahl, B.L.S. Maddux, J.E. Hutchison, Chem. Rev. 107 (2007) 2228–2269.
[17] B. Ruiz-Camacho, M.A. Valenzuela1, J.A. Perez-Galindo, F. Pola, M. Miki-Yoshida, N. Alonso-Vante, R.G. Gonzalez-Huerta, J. New Mater. Electrochem. Systems 13 (2010) 183–189.
[18] B. Ruiz-Camacho, R.G. Gonzalez-Huerta, M.A. Valenzuela, N. Alonso-Vante, Top. Catal. 54 (2011) 512–518.
[19] A. Peled, N. Mirchin, Photo-Excited Processes Diagnostics and Applications, Kluwer Academic Publishers, Netherlands, 2003, 251–280.
[20] C. Crisafulli, S. Sciré, S. Giuffrida, G. Ventimiglia, R. Lo Nigro, Appl. Catal. A: Gen. 306 (2006) 51–57.
[21] S. Giuffrida, F.F. Condorelli, L.L. Costanzao, G. Ventimiglia, J. Nanopart. Res. 19 (2007) 611–619.
[22] S. Scirè, C. Crisafulli, S. Giuffrida, G. Ventimiglia, C. Bongiorno, C. Spinella, J. Mol. Catal. A: Chem. 333 (2010) 100–108.
[23] J.C. Scaiano, P. Billone, C.M. Gonzalez, L. Maretti, M:l. Marin, K.L. McGilvray, N. Yuan, Pure Appl. Chem. 81 (2009) 635–647.
[24] M. Sakamoto, M. Fujistuka, T. Majima, J. Photochem. Photobiol. C. Photochem. Rev. 10 (2009) 33–56.
[25] M. Cerro-Alarcón, B. Bachiller-Baeza, A. Guerrero-Ruiz, I. Rodríguez-Ramos, J. Mol. Catal. A: Chem. 258 (2006) 221–230.
[26] B. Zapata, M.A. Valenzuela, J. Palacios, E. Torres-Garcia, Int. J. Hydrogen Energy 35 (2010) 12091–12097.
[27] F. Forouzan, C.T. Richard, J.A. Bard, J. Phys. Chem. 100 (1996) 18123–18127.
[28] V. Iliev, D. Tomova, L. Bilyarska, G. Tyuliev, J. Mol. Catal. A: Chem. 263 (2007) 32–38.
[29] A. Mills, M.A. Valenzuela, J. Photochem. Photobiol. A. Chem. 165 (2004) 25–34.
[30] M. Alvarez Lemus, T. López, S. Recillas, D.M. Frías, M. Montes, J.J. Delgado, M.A. Centeno, J.A. Odriozola, J. Mol. Catal. A: Chem. 281 (2008) 107–112.
[31] S. Velu, S.K. Gangwal, Solid State Ionics 177 (2006) 803–811.
[32] I.K. Konstantinou, T.A. Albanis, Appl. Catal. B: Environ. 49 (2004) 1–14.
[33] Y.L. Chow, G.E. Buono–Core, C.W.B. Lee, J.C. Scaiano, J. Am. Chem. Soc. 108 (1986) 7620–7627.
[34] T. Sato, H. Onaka, Y. Yonezawa, J. Photochem. Photobiol. A: Chem. 127 (1999) 83–87.
[35] Y. Yonezawa, T. Sato, S. Kuroda, J. Chem. Soc. Faraday Trans. 87 (1991) 1905–1910.
[36] I. Preda, L. Soriano, L. Alvarez, J. Mendez, F. Yubero, A. Gutierrez, J.M. Sanz, Surf. Interf. Anal. 42 (2010) 869–873.
[37] S. Scirè, S. Giuffrida, C. Crisafulli, P.M. Riccobene, A. Pistone, J. Nanopart. Res. 13 (2011) 3217–3228.
[38] H.S. Nalwa (Ed.), Handbook of Photochemistry and Photobiology, V-1, Inorganic Photochemistry, American Scientific Publishers, 2003.
[39] S.M. Avramescu, C. Bradu, I. Udrea, N. Mihalache, F. Rurta, Catal. Commun. 9 (2008) 2386–2391.
[40] J. Li, Y. Lu, Q. Ye, M. Cinke, J. Han, M. Meyyappan, Nano Lett. 3 (2003) 929–933.
[41] S. Suzuki, Y. Watanabe, T. Ogino, S. Heun, L. Gregoratti, A. Barinov, B. Kaulich, M. Kiskinova, W. Zhu, C. Bower, O. Zhou, Phys. Rev. B 66 (2002) 035414–035418.
[42] H. Ago, T. Kugler, F. Cacialli, W.R. Salaneck, M.S.P. Shaffer, A.H. Windle, R.H. Friend, J. Phys. Chem. B 103 (1999) 8116–8121.
[43] N. Kruse, S. Chenakin, Appl. Catal. A: Gen. 391 (2011) 367–376.
[44] L. Soriano, I. Preda, A. Gutiérrez, S. Palacín, M. Abbate, A. Vollmer, Phys. Rev. B 75 (2007) 233417–233420.
[45] A.R. González, J.P. Holgado, R. Álvarez, G. Munuera, J. Phys. Chem. 96 (1992) 3080–3086.
[46] N.V. Smirnova, T.B. Boitsova, V.V. Gorbunova, L.V. Alekseeva, V.A. Pronin, G.S. Konuhov, Thin Solid Films 513 (2006) 25–30.
[47] J.J. Zou, C.J. Liu, Y.P. Zhang, Langmuir 22 (2006) 2334–2339.
[48] S. Xing, C. Hu, J. Qu, H. He, M. Yang, Environ. Sci. Technol. 42 (2008) 3363–3368.
[49] C. Hu, S. Xing, J. Qu, H. He, J. Phys. Chem. C 112 (2008) 5978–5983.
[50] R.R. Giri, H. Ozaki, R. Takanami, S. Taniguchi, Water Sci. Technol. 58 (2008) 207–216.
[51] E. Brillas, J.C. Calpe, P.L. Cabot, Appl. Catal. B: Environ. 46 (2003) 381–391.